NJC

ROYAL SOCIETY OF CHEMISTRY

PAPER

View Article Online
View Journal

Cite this: DOI: 10.1039/d0nj05323f

V-shaped fluorophores with a 1-methyl-4,5-bis(arylethynyl)imidazole skeleton displaying solid-state fluorescence, acid responsiveness, and remarkable fluorescence solvatochromism†

Youhei Miura, * Kotaro Kobayashi and Naoki Yoshioka

Received 30th October 2020,
Accepted 3rd December 2020

DOI: 10.1039/d0nj05323f

rsc.li/njc

Novel V-shaped fluorophores with an imidazole skeleton composed of arylethynyl moieties were developed. Their HOMO–LUMO energy gaps were well controlled by the introduction of electron-withdrawing or -donating groups in the aryl moiety. Compounds with different substituents at the 4- and 5-positions were selectively synthesized exploiting the difference in reactivity between the iodo and bromo groups. All compounds synthesized displayed fluorescence not only in solution but also in the solid state. The compound with a donor–acceptor structure displayed a fluorescence maximum with a wavelength over 500 nm and a large Stokes shift of about 150 nm, due to its intramolecular charge transfer character. In the solid state, the synthesized compounds have planar structures, indicating an expansion of π-conjugation. Upon exposure of the compounds in the solid state to acid vapor, the fluorescence of the compounds with acceptor groups was quenched, and that of the others shifted to longer wavelengths.

Introduction

Fluorescent organic compounds have attracted much research attention, as they are used in various applications in the fields of functional materials and bio-probes.[1] Organic fluorophores are often characterized by large π-conjugated skeletons like naphthalene, pyrene, perylene, and azaacene.[2,3] These skeletons are especially desirable in fluorophores, because they have fluorescence properties themselves; furthermore, substituents introduced in these skeletons may act as auxochromes. Notably, however, large π-conjugate systems often display a tendency toward aggregation, which may induce fluorescence quenching.[4] Therefore, fluorophores characterized by small π-conjugate structures represent desirable target compounds when designing fluorescent functional materials. Imidazole is one of the smallest neutral aromatic compounds; it has both hydrogen-bond-donating and hydrogen-bond-accepting characters, as well as an ability to form coordination bonds. These features have often been exploited in the construction of supramolecular species and to obtain proton-conducting materials.[5] Nevertheless, few reports have been published on fluorescent dyes containing the imidazole moiety in the absence of annulation,[6] although several annulated imidazole derivatives, such as phenanthroimidazole[7] and pyridoimidazole,[8] have been reported as organic fluorophores. In fact, the extent of π-conjugation is limited in imidazole, and this compound is not fluorescent on its own. However, as in the case of 2,4,5-triphenylimidazole, known as lophine,[9] which has been found to be chemoluminescent and fluorescent,[10] the imidazole skeleton can be made to acquire fluorescence properties *via* the introduction of appropriate substituents.

The carbon atoms in the 4- and 5-positions of imidazole are characterized by different electronic densities (Scheme 1), because the nitrogen atoms linking them are of different types; one is a sp^3 hybridization, whereas the other is imine-type sp^2 hybridization. Although the electron density of the highest occupied molecular orbital (HOMO) at C4 is almost equal to that at C5, the electron density of the lowest unoccupied molecular orbital (LUMO) is three times larger at C5 than that at C4. Nevertheless, the differences between these carbon atoms are often not taken into consideration, as imidazole easily isomerizes in solution *via* hydrogen migration. Notably, placing a substituent on the nitrogen at the 1-position of imidazole is the easiest way to prevent the mentioned isomerization. This synthetic transformation does not affect the atomic orbital coefficients of HOMO and LUMO in imidazole and allows the difference in the electronic states between C4 and C5 to be observed. However, the high-selectivity synthesis of

Department of Applied Chemistry, Faculty of Science and Technology, Keio University, Yokohama, 223-8522, Japan. E-mail: y-miura@applc.keio.ac.jp

† Electronic supplementary information (ESI) available: Synthetic method, analytical and spectral data, and details of computational data are available. CCDC 1950075 (**1a**), 1950076 (**1b**), 2025902 (**1c**), 1950078 (**1d**), 1950077 (**1e**), 2025951 (**1a-TFA salt**), 2025950 (**1d-TFA salt**) and 2025952 (**1e-TFA salt**). For ESI and crystallographic data in CIF or other electronic format see DOI: 10.1039/d0nj05323f

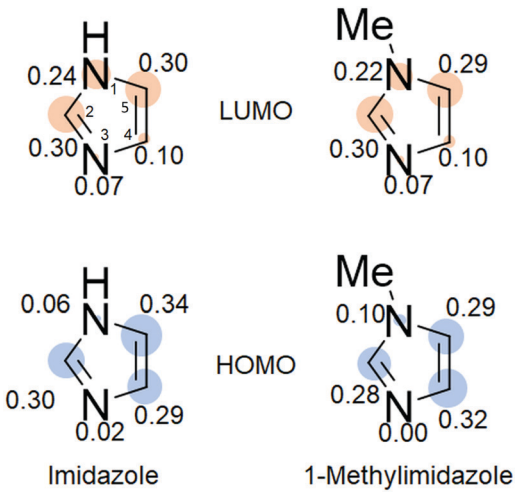

Scheme 1 Atomic orbital coefficients of the frontier orbitals of imidazole and 1-methylimidazole calculated using the PM3 method.

substituted imidazoles is hard to achieve using the classical synthetic strategy, which consists of the condensation between an aldehyde, a 1,2-diketone, and ammonia.[11] Recently, cross-coupling reactions involving haloimidazoles have been reported, which enable the organic chemists to selectively introduce the desired substituent in the 4- and 5-positions of the substrate.[12] Several 4,5-disubstituted imidazole derivatives could be selectively synthesized using this approach, expanding the scope of synthetically accessible imidazole-based functional materials.

In the present study, 4,5-bis(arylethynyl)imidazole, a family of novel small fluorophores with V-shaped structures, was designed with the aim of exploiting the characteristic electronic state of the imidazole skeleton (Scheme 2). In the D–π–A molecule, the V-shaped structure spatially separates the HOMO and LUMO, which have localized electron density. This structure is suitable for fluorescence solvatochromism of molecules.[13] The arylethynyl group is widely used for the functionalization of compounds like pyrene and perylene to obtain fluorophores.[14] This group expands the π-conjugation of the substrate while increasing its bulkiness only modestly; additionally, the arylethynyl group is stable, and it is easily introduced into the aryl skeleton *via* Sonogashira coupling. Notably, the substitution effects on the aryl rings of 4,5-diarylethynylimidazole were estimated by performing density functional theory (DFT) calculations. Moreover, the fluorescence and absorption properties of the compounds synthesized in the present study (Scheme 2) were analyzed both in the solid state and in solution. These compounds were also studied as acid vapor detectors in the solid state.

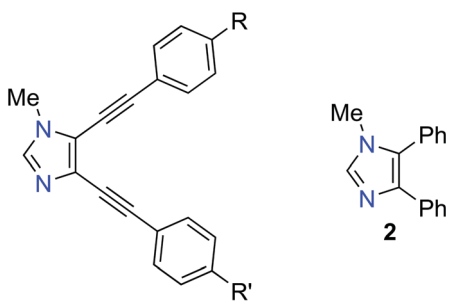

Scheme 2 Molecular structures of compounds **1a–e** and **2**.

Results and discussion

Molecular design

DFT calculations (at the B3LYP/6-311(d) level of theory) were performed to predict the effect of the introduction of various aryl ethynyl substituents in imidazole. In particular, the frontier orbital energies of 4,5-bis(phenylethynyl)-1-methylimidazole (**1a**), 4,5-bis(4-methoxyphenylethynyl)-1-methylimidazole (**1b**), 4,5-bis(4-formylphenylethynyl)-1-methylimidazole (**1c**), 4-phenylethynyl-5-(4-formylphenylethynyl)-1-methylimidazole (**1d**), and 4-(4-methoxyphenylethynyl)-5-(4-formylphenylethynyl)-1-methylimidazole (**1e**) were calculated (Fig. 1 and Fig. S1, ESI†). Structure optimization indicated all compounds to be planar, with small torsion angles existing between the imidazole and aryl rings (Tables S1–S5, ESI†). Compound **1a** was estimated to have a higher HOMO energy, lower LUMO energy, and smaller HOMO–LUMO energy gap (3.70 eV) than those of 4,5-diphenyl-1-methylimidazole (**2**) (4.65 eV), owing to the π-conjugation extension and the planarization of the phenyl rings resulting from the introduction of the ethynylene groups. The introduction of the methoxy groups to produce **1b** was associated with mutually similar increases in the energies of the HOMO and LUMO; therefore, the HOMO–LUMO energy gap calculated for **1b** (3.62 eV) was almost the same as that calculated for **1a**. In contrast, the introduction of the electron-withdrawing formyl groups (to produce compound **1c**) caused the calculated value of the HOMO–LUMO energy gap to decrease (3.22 eV). This result was due to a decrease in the LUMO energy (ΔE(**1c–1a**) = −0.98 eV) that was larger than that of its counterpart for HOMO (ΔE(**1c–1a**) = −0.49 eV). The introduction of a single formyl group to produce derivative **1d** was associated with a decrease in the HOMO and LUMO energies with

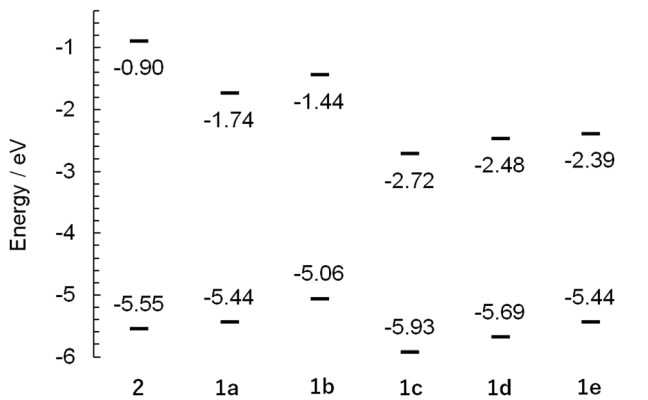

Fig. 1 Energy diagram of the frontier orbitals of compounds **2** and **1a–e**.

respect to **1a**, although both energies were higher than those of their counterparts for **1c**. The HOMO–LUMO energy gap of **1d** was calculated to be 3.21 eV, a value almost identical to that calculated for **1c**. Furthermore, introduction of a methoxy group at the R′ position of **1d** (to produce compound **1e**) induced an increase in the energy of the HOMO, whereas the LUMO energy was hardly modified. This molecule displayed the smallest calculated HOMO–LUMO energy gap (3.05 eV) among the compounds in the **1a–e** series. According to calculations, the electron densities of the HOMO and LUMO of **1e** mainly distribute on the methoxyphenylethynyl group and the formylphenylethynyl group, respectively. A similar distribution of HOMO and LUMO electron densities was observed for **1d**. Notably, such large differences between HOMO and LUMO atomic orbital coefficients often result in an intramolecular charge transfer (ICT).

The results of DFT calculations suggest that the introduction of electron-donating groups in the R and R′ positions of the imidazole derivatives described above does not affect the HOMO–LUMO energy gap, even though the individual energies of the HOMO and LUMO increase as a consequence of the modification. Although the introduction of electron-withdrawing groups in the mentioned positions cause a decrease in both the HOMO and LUMO energies, the decrease is more substantial for the LUMO than for the HOMO. Furthermore, the introduction of an electron-withdrawing group in the R position is associated with a decrease in the HOMO–LUMO energy gap. Finally, the concomitant introduction of an electron-withdrawing group in the R position and an electron-donating group in the R' position results in the formation of a donor–acceptor structure and of a compound displaying a small HOMO–LUMO energy gap. This result is well explained by the difference in the atomic orbital coefficient between the C4 and C5 positions of the imidazole unit illustrated in Scheme 1, according to which the electron density of the LUMO is low at the 4-position.

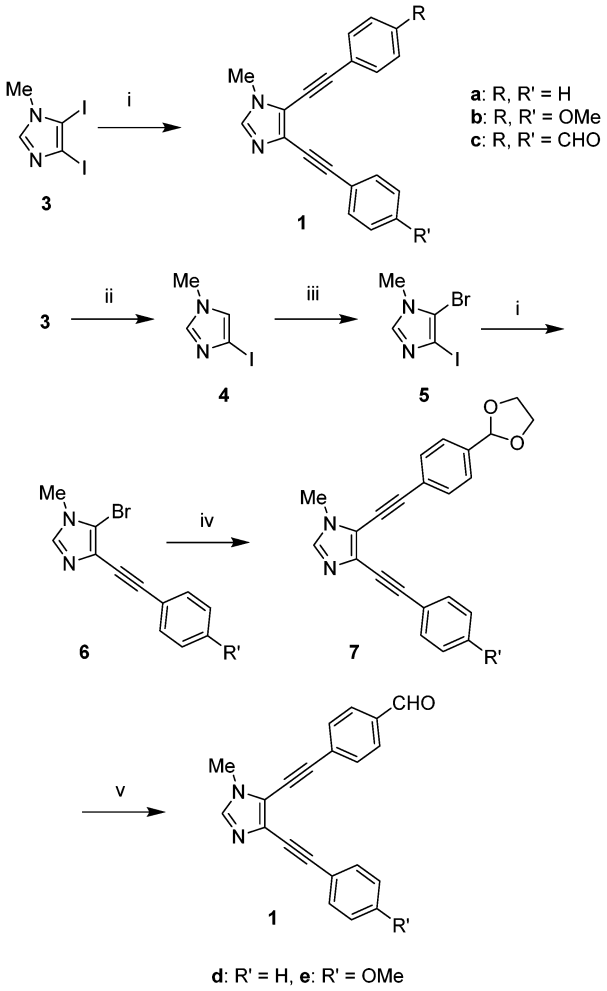

Scheme 3 Synthesis of compound **1**. Reagents and conditions: (i) arylacetylene, $Pd(PPh_3)_2Cl_2$, triethylamine (NEt_3), dimethylformamide (DMF), r.t.; (ii) iPrMgBr, tetrahydrofuran (THF), 0 °C; (iii) *N*-bromosuccinimide, THF, room temperature (r.t.); (iv) 2-(4-ethynylphenyl)dioxolane, $Pd(PPh_3)_2Cl_2$, NEt_3, DMF, 90 °C; and (v) 1 M HCl, acetone, r.t.

Syntheses

Species containing identical arylethynyl groups as substituents (compounds **1a–c**) were synthesized by performing Sonogashira coupling[15,16] between 4,5-diodo-1-methylimidazole **3** and the relevant arylacetylene. Compounds **1d** and **1e** were synthesized using a two-step Sonogashira coupling (Scheme 3) using 5-bromo-4-iodo-1-methylimidazole (**5**) and exploiting the difference in reactivity between the Br and I substituents.[12b] In particular, compound **5** was prepared by the selective deiodination of **3**[17] using a Grignard reagent followed by a bromination step. The Sonogashira coupling between **5** and phenylacetylene at room temperature produced 5-bromo-4-phenylethynyl-1-methylimidazole (**6d**), selectively. Notably, a Sonogashira coupling between **6d** and 4-ethynylbenzaldehyde was attempted at 90 °C, but the target compound **1d** was not obtained. Therefore, 2-(4-ethynylphenyl)-1,3-dioxolane, in which 4-ethynylbenzaldehyde is protected by ethylene glycol, was used in the Sonogashira coupling with **6d**. This reaction produced **7** in moderate yield and, following deprotection, **1d** in good yield. The methoxy- and formyl-substituted compound **1e** was synthesized in just the same manner as described for **1d**.

Spectroscopic properties in solution

The absorption spectra of compounds **1a–e** were measured in CH_2Cl_2 (Fig. 2 and Table 1). All compounds displayed two dominant absorptions: a relatively sharp absorption with a maximum at 270–290 nm and a broad absorption with a maximum at 330–370 nm. Focusing on the longer wavelength absorptions, which are due to the HOMO–LUMO transition, **1a** and **1b** displayed maxima near 330 nm, whereas **1c–e**, which comprise formyl groups, displayed maxima near 370 nm. The absorption edges of **1a–e** are observed at 363, 368, 413, 407, and 418 nm, respectively, and the values of their optical band gaps were calculated to be 3.42, 3.37, 3.00, 3.05, and 2.97 eV, respectively. These results match the results of the DFT calculations, according to which the introduction of the formyl group induces a decrease in the HOMO–LUMO energy gap, whereas the introduction of methoxy groups has little influence on it.

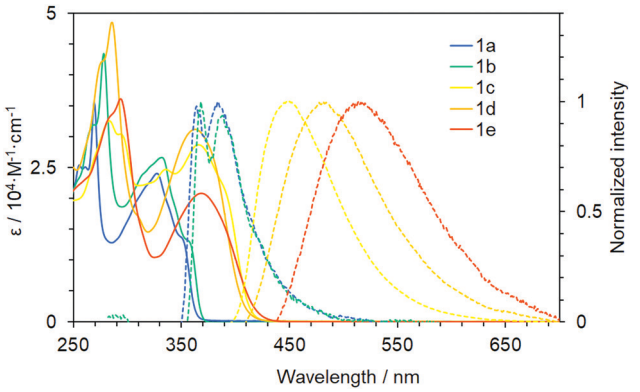

Fig. 2 Absorption and fluorescence spectra of compounds **1a** (1.24×10^{-5} M), **1b** (1.6×10^{-5} M), **1c** (1.3×10^{-5} M), **1d** (1.4×10^{-5} M), and **1e** (1.4×10^{-5} M). The excitation wavelengths are the compounds' λ_{abs} (solid line: absorption spectra, dashed line: fluorescence spectra).

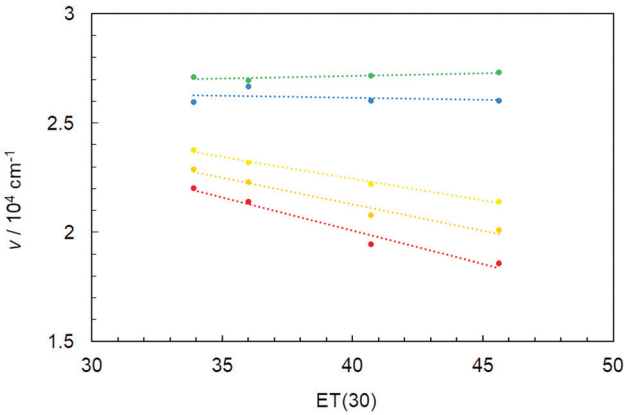

Fig. 3 Correlation between solvent polarity and fluorescence maximum wavenumber. Blue: **1a**; green: **1b**; yellow: **1c**; orange: **1d**; and red: **1e**. ET(30): solvent polarity parameter.

The fluorescence spectra of **1a** and **1b** in CH_2Cl_2 are similar to each other (Fig. 2). These spectra display fluorescence maxima at about 365 and 385 nm. Compounds **1c–e** displayed fluorescence maxima at longer wavelengths than compounds **1a** and **1b**, similar to what had been observed in the absorption spectra. However, the fluorescence maxima of **1c–e** are quite different from each other, as opposed to what had been observed in the absorption spectra. Compound **1c**, which has two formyl substituents, displayed a fluorescence maximum at 450 nm in CH_2Cl_2. Compound **1d**, which has a single formyl group at the R position, displayed a fluorescence maximum at 481 nm. Compound **1e**, which has a methoxy substituent and a formyl substituent, displayed a fluorescence maximum at 514 nm, the longest wavelength in the **1a–e** series. In summary, the fluorescence spectrum of **1e** is characterized by a large Stokes shift (146 nm). The wavelength differences between the fluorescence maxima in the **1c–e** series can be explained by the existence of an ICT. In **1d** and **1e**, the electron density of the HOMO is distributed around the phenyl ethynyl or methoxyphenylethynyl and imidazole moiety, whereas that of the LUMO is mainly distributed around the formylphenylethynyl moiety. The large difference in the atomic orbital coefficient between the HOMO and LUMO results in a difference in the dipole moment between the ground and excited states, causing an ICT to be observed. The electron density localization of HOMO and LUMO progressively decreases on going from **1e** to **1d** and to **1c**, as a consequence of the difference in the electron-donating properties of the substituents in the R′ position. Therefore, the ICT character of the electronic transition is suggested to increase in strength on going from **1e** to **1d** and to **1c**. In many cases, fluorophores with ICT character show remarkable fluorescence solvatochromism.[18]

Notably, the fluorescence spectra of **1a–e** were also recorded in toluene, 1,4-dioxane, and CH_3CN solutions (Fig. S2, ESI†). The spectrum of compound **1e** displayed an 84 nm shift in wavelength of the emission maximum when the solvent was switched from toluene to CH_3CN. The wavelength shifts displayed by **1c** and **1d** under the same conditions were 46 and 60 nm, respectively. In contrast, **1a** and **1b** displayed only small fluorescence solvatochromism. The correlation between the solvent polarity parameter (ET(30)) and the fluorescence wavenumber is often used to compare the fluorescence solvatochromism properties of compounds (Fig. 3).[19] The steeper the slope of the curve of the fluorescence wavenumber *versus* ET(30), the brighter the solvatochromism. The slopes of the mentioned curves measured for compounds **1a–e** are 19, −25, 199, 243, and 306 cm^{-1}, respectively. These results indicate that the fluorescence solvatochromic properties increased in the following order: **1b** ≅ **1a** < **1c** < **1d** < **1e**. This evidence also supports the order of strength of the ICT character in the electronic transition.

Table 1 Absorption and fluorescence features of compounds **1a–e**

Compound	λ_{abs}[a]/nm	ε[a]/10^4 M^{-1} cm^{-1}	$\lambda_{em,sol}$/nm (Φ_{sol}[b])				$\lambda_{em,cry}$/nm (Φ_{cry}[b])
			Toluene	1,4-Dioxane	CH_2Cl_2	MeCN	
1a	327	2.41	385 (0.05)	375 (0.06)	384 (0.03)	384 (0.03)	405 (0.22)
1b	332	2.70	369 (0.01)	371 (0.09)	368 (0.007)	366 (0.004)	396 (0.07)
1c	366	2.86	421 (0.06)	431 (0.07)	450 (0.20)	467 (0.07)	551 (0.05)
1d	363	3.13	437 (0.04)	448 (0.04)	481 (0.07)	497 (0.02)	498 (0.28)
1e	368	2.05	454 (0.06)	467 (0.04)	514 (0.03)	538 (0.008)	523 (0.25)

Excitation wavelengths are λ_{abs} for all compounds. λ_{abs}: absorption maximum over 300 nm. ε: molar absorption ecoefficiency. $\lambda_{em,sol}$: fluorescence maximum in solution. Φ_{sol}: quantum yield in solution. $\lambda_{em,cry}$: fluorescence maximum in the solid state. Φ_{cry}: quantum yield in the solid state. [a] Values were measured in CH_2Cl_2. [b] Absolute quantum yields were determined employing the integrating sphere system.

Solid-state properties

All compounds displayed fluorescence in the solid state (Fig. 4 and Fig. S3, ESI†). The wavelengths of the fluorescence maxima of **1a**, **1b**, **1d**, and **1e** were 405, 396, 498, and 523 nm, respectively. The differences in the wavelengths of the fluorescence maxima of **1a**, **1d**, and **1e** between solid state and solution were relatively small. However, the wavelengths of the fluorescence maxima of **1b** and **1c** in the solid state were 30 and 100 nm longer than that in solution, respectively.

Although the fluorescence quantum yields of **1a–e** in solution were relatively low, in the solid state, the values of these parameters were moderately high. This observation is the result of the suppression of molecular motions in the crystal phase.

Notably, compounds **1a–e** produced single crystals that were suitable for X-ray structural analysis (Fig. 5 and Table S6, ESI†).[20] Four crystallographically independent molecules were observed in the **1a** crystal. The largest torsion angle between the imidazole ring and the aryl ring was observed in compound **1b** (44°). The corresponding torsion angles for the other compounds were about 25°, meaning that all these compounds had a relatively planar structure.

Three major intermolecular contacts *via* π-orbitals were observed in the crystals of compounds **1a–e**. The first is an antiparallel π-stacking between the arylethynylimidazole moieties observed in **1a**, **1c**, and **1d** (contact A, Fig. 6a). The second is an antiparallel imidazole–imidazole stacking observed in **1a** and **1e** (contact B, Fig. 6b). The third is a π-stacking between the aryl ring and imidazole ring observed in **1b** and **1c** (contact C, Fig. 6c). Additionally, molecular contact *via* aryl rings was observed in the crystal of **1c** (contact D, Fig. 6d). The shortest distances between atoms in all contacts were in the range of 3.4–3.6 Å. Contact C observed in **1b** and **1c** is similar to a J-aggregate-type structure, suggesting a small excitation energy. Excitation energies of those dimeric structures of **1b** and **1c** were calculated by implementing the time-dependent DFT method (Tables S7 and S8, ESI†). The oscillator strength of the HOMO–LUMO excitation of contact A and D was calculated to have a value of 0 for both **1b** and **1c**, suggesting a forbidden transition. Meanwhile, those of contact C in compounds **1b** and **1c** were calculated to be 0.518 and 0.0283, respectively. In **1c**, the excitation energies of the dimer of contact C and monomer were calculated to have values of 2.92 and 3.12 eV, respectively. Therefore, the excitation energy decreased by about 0.2 eV as a result of the formation of the π-stacked dimer. Similarly, the energy change associated with **1b** dimer formation was calculated to be about 0.055 eV. Similar results were obtained in the contact C trimer structure (Tables S9 and S10, ESI†). These calculation results are in agreement with experimental results.

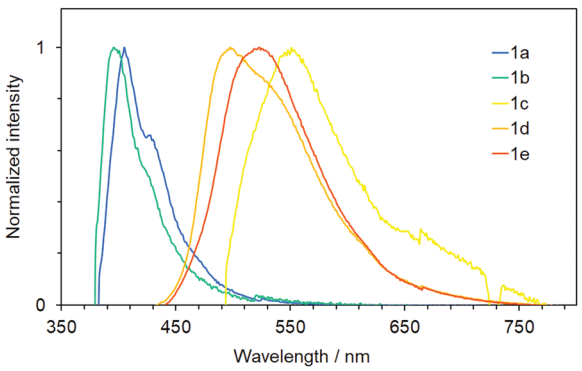

Fig. 4 Fluorescence spectra of compounds **1a–e** in the solid-state.

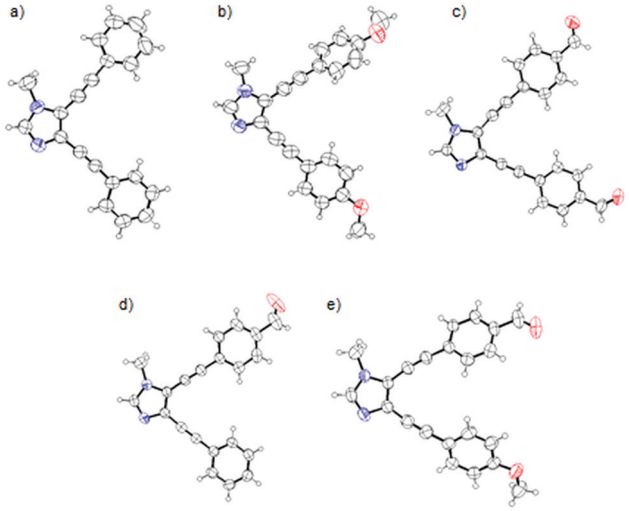

Fig. 5 Crystal structures of (a) **1a**, (b) **1b**, (c) **1c**, (d) **1d**, and (e) **1e**.

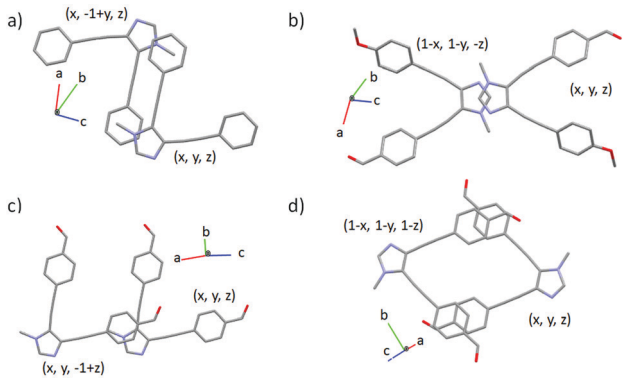

Fig. 6 Molecular packing in the crystal. (a) Antiparallel π-stacking between arylethynylimidazole moieties in **1a** (contact A). (b) Antiparallel imidazole–imidazole stacking in **1e** (contact B). (c) π-Stacking between the aryl ring and imidazole ring in **1c** (contact C). (d) Molecular contact *via* aryl rings in **1c** (contact D).

Acid responsiveness

The response of compounds **1a–e** to acid vapor was examined in the solid state, relying on the basicity of the imidazole skeleton (Fig. 7 and Fig. S4, ESI†). Notably, the binding of a proton to the nitrogen atom in the 3-position of the imidazole moiety caused remarkable changes in the electronic structure and spectroscopic properties of the compounds. After single crystals of compounds **1a–e** were exposed to hydrochloric acid vapor, their fluorescence properties underwent substantial modifications, even though the colors of the samples changed

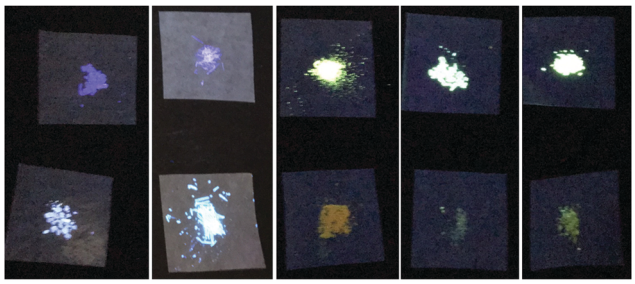

Fig. 7 Photographs of compounds **1a–e** in the solid state under UV light (365 nm) irradiation. The photographs above were taken before the exposure of compounds to acid vapor, the ones below were taken after exposure to acid vapor.

only slightly. These acid responses are irreversible. The fluorescence of compounds **1c–e**, the electronic transitions of which have ICT character, was quenched after the compounds were exposed to the acid vapor for about 10 s. Meanwhile, following exposure to hydrochloric acid vapor, **1a** and **1b** displayed weak fluorescence, with quantum yields of about 0.01 and 0.03, respectively. Additionally, the fluorescence maximum of **1b** was observed at 453 nm, meaning that this peak shifted toward longer wavelengths with respect to the neutral crystal.

The effects of adding trifluoroacetic acid (TFA) to the solutions of compounds **1a–e** were also examined (Fig. 8).[21] The quantum yields of compounds **1a** and **1b** increased as a result of the addition of TFA. In contrast, the fluorescence of compounds **1c–e** was quenched or weakened. In other words, the fluorescence of compounds, the electronic transitions of which had an ICT character, was weakened by the addition of TFA in solution. This tendency is similar to that observed in the acid vapor exposure experiments. The fluorescence spectra of **1a** and **1b** solutions recorded following TFA addition display two maxima. The fluorescence spectrum of **1a** after TFA addition is similar to that of **1a**

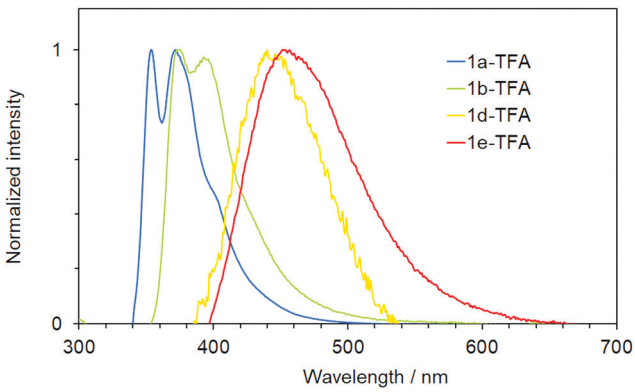

Fig. 8 Fluorescence spectra of **1a**, **1b**, **1d**, and **1e** in CH_2Cl_2 solution in the presence of excess trifluoroacetic acid, **1a** (Φ = 0.33, λ_{ex} = 327 nm, 1.24 × 10^{-5} M); **1b** (Φ = 0.34, λ_{ex} = 332 nm, 1.6 × 10^{-5} M); **1d** (Φ = 0.01, λ_{ex} = 363 nm, 1.4 × 10^{-5} M); and **1e** (Φ = 0.03, λ_{ex} = 368 nm, 1.4 × 10^{-5} M). Please note that compound **1c** displayed no fluorescence. Φ: fluorescence quantum yield; λ_{ex}: excitation wavelength.

recorded in the absence of TFA. The fluorescence maxima of **1b** (374 and 393 nm) shifted to longer wavelengths as a result of the addition of TFA. In contrast, adding TFA to solutions of **1d** and **1e** caused their fluorescence maxima to shift toward shorter wavelengths (440 and 452 nm, respectively). Notably, adding TFA to the solution of the mentioned compounds triggered the formation of imidazolium species. In the case of **1b**, as a consequence of imidazolium formation, a donor–acceptor system formed between the anisyl moieties and the imidazolium moieties (Fig. S5, ESI†). In the case of **1d** and **1e**, the length between donor and acceptor becomes shorter due to imidazolium formation. These changes in electronic structure caused the fluorescence spectra of these compounds to shift toward different wavelengths. Similar spectroscopic changes resulting from imidazolium formation have been reported in the study of 1,1′-diaryl-2,2′-biimidazole derivatives.[21b]

Single crystals of TFA salts of **1a**, **1d**, and **1e** were obtained by recrystallization (Fig. 9).[20,22] All these molecules were characterized by a planar structure with small torsion angles (<20°) between the imidazole and aryl rings. In all three molecules, the nitrogen in the 3-position of the imidazole ring was in contact with one oxygen of the trifluoroacetate anion (~2.6 Å). The crystal of the TFA salt of **1d** comprises two crystallographically independent molecules, and it contains 1/2 molecule of neutral TFA per one of **1d** salt; notably, the neutral TFA molecule is in contact with the trifluoroacetate anion. In contrast to the crystals of the neutral species, the crystals of all TFA salt derivatives displayed stacked structures along the π direction. Molecules form a slip-stacked structure in the crystals of the salts of both **1a** and **1d**. In the crystal of the TFA salt of **1e**, the

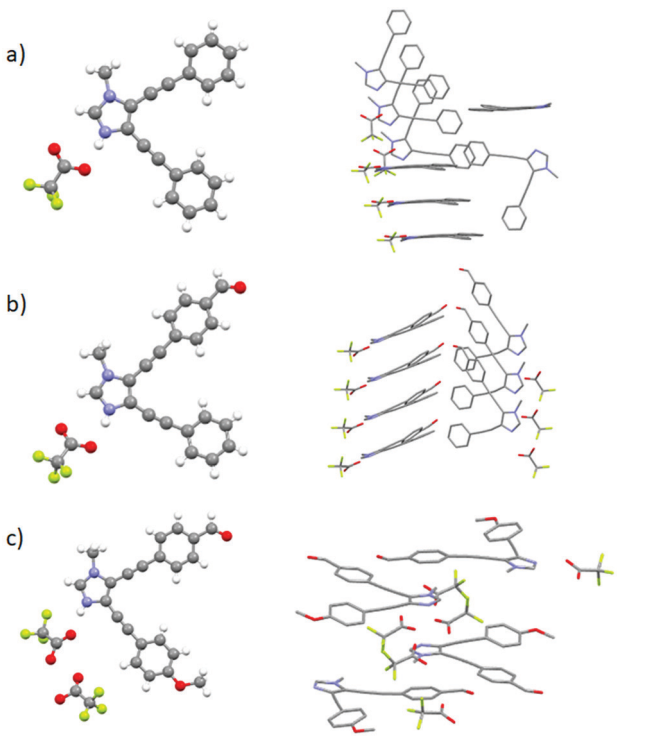

Fig. 9 Crystal structures and molecular arrangements of trifluoroacetate salts of (a) **1a**, (b) **1d**, and (c) **1e**.

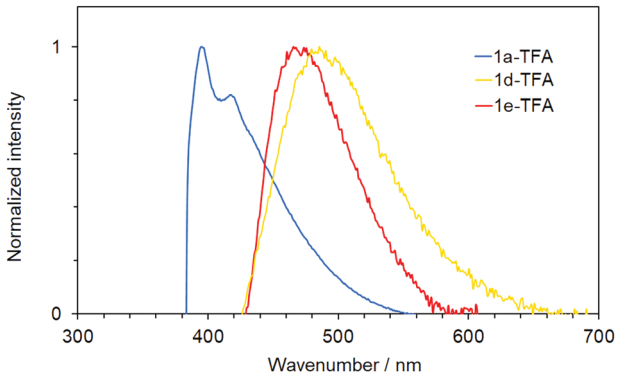

Fig. 10 Fluorescence spectra of the trifluoroacetate salts of **1a** (Φ = 0.13, λ_{ex} = 372 nm), **1d** (Φ = 0.03, λ_{ex} = 412 nm), and **1e** (Φ = 0.06, λ_{ex} = 418 nm) in crystalline form.

formylphenyl and imidazolium moieties overlap each other, so that they are at a distance of about 3.45 Å.

The fluorescence maxima of the crystals of the TFA salts of **1a** and **1d** (395 and 486 nm, respectively) appeared at longer wavelengths than that of their counterparts observed for salts of **1a** and **1d** in solution (Fig. 10). The crystal of **1e** salt displayed a similar fluorescence maximum (465 nm) to that observed for **1e** salt in solution. The shifts to longer wavelengths of the fluorescence maxima of the TFA salts of **1a** and **1d** in crystalline phase with respect to that of their counterparts for salts of **1a** and **1d** in solution are due to the formation of J-aggregation-type structures, similar to those observed for the relevant neutral compounds in the solid state.

Conclusions

Novel V-shaped imidazole-based small fluorophores comprising arylethynyl groups were designed and synthesized. Introducing arylethynyl groups in the 4- and 5-positions of the imidazole skeleton effectively modified the values of the HOMO and LUMO energies and caused the resulting compounds to display fluorescence. These compound electronic structures matched quite well with those predicted based on DFT calculations. These compounds displayed moderate quantum yields not only in solution but also in the solid state. Compounds **1c–e**, which comprise formyl substituents, displayed ICT properties as well as remarkable fluorescence solvatochromism. In particular, in CH_2Cl_2 solution, the methoxy- and formyl-substituted **1e** displayed a fluorescence maximum at a wavelength of over 500 nm and a large Stokes shift of about 150 nm. Upon exposure of **1a** and **1b** in the solid state to acid vapor, the fluorescence maxima of these compounds shifted to longer wavelengths. In the corresponding experiments, the fluorescence of compounds **1c–e** was quenched. The fluorescence maximum of **1b** in a solution to which acid had been added appeared at a longer wavelength than that of its counterpart to which no acid had been added. In contrast, the fluorescence maxima of **1d** and **1e** in acid-added solution appeared at a shorter wavelength than that of the corresponding neutral solution. These results can be explained by changes in their D–π–A structure. In the solid state, the formation of J-aggregate-type stacked structures observed in **1b**, **1c**, TFA salt of **1a**, and TFA salt of **1d** induced a long-wavelength shift of the fluorescence maxima in both neutral and imidazolium species.

Experimental section

UV-Vis absorption spectra were measured using a JASCO V-650 instrument. Fluorescence spectra and quantum yields were measured using a SHIMADZU RF-6000 system with integral sphere attachment. X-ray crystal structure analysis was performed using a Bruker D8 VENTURE instrument and APEX3 application. DFT calculations were performed by Gaussian 09 revision D.01.[23] All purchased reagents and solvents were used without further purification. NMR spectra were measured using JEOL JNM-ECS-400, JEOL JNM-ECZ-400s, or JEOL JNM-LA-300 instruments. Mass spectrometry was performed using a Waters LCT-Premier (high-resolution, ESI) instrument. IR spectra were recorded using a JASCO FT/IR-4100 system. All IR measurement were performed using the KBr method. Synthetic details and characterizations are described in the ESI.†

Conflicts of interest

There are no conflicts to declare.

Acknowledgements

This work was partly supported by Keio Gijuku Academic Development Funds.

Notes and references

1 (*a*) M. Shimizu and T. Hiyama, *Chem. – Asian J.*, 2010, **5**, 1516–1531; (*b*) R. Hu, N. L. C. Leungb and B. Z. Tang, *Chem. Soc. Rev.*, 2014, **43**, 4494–4562; (*c*) M. Y. Wong and E. Zysman-Colman, *Adv. Mater.*, 2017, **29**, 1605444.

2 (*a*) M. A. Kobaisi, S. V. Bhosale, K. Latham, A. M. Raynor and S. V. Bhosale, *Chem. Rev.*, 2016, **116**, 11685–11796; (*b*) T. M. Figueira-Duarte and K. Müllen, *Chem. Rev.*, 2011, **111**, 7260–7314; (*c*) N. Soh and T. Ueda, *Talanta*, 2011, **85**, 1233–1237; (*d*) F. Würthner, C. R. Saha-Möller, B. Fimmel, S. Ogi, P. Leowanawat and D. Schmidt, *Chem. Rev.*, 2016, **116**, 962–1052.

3 (*a*) R. Suzuki, R. Tada, T. Hosoda, Y. Miura and N. Yoshioka, *New J. Chem*, 2016, **40**, 2920–2926; (*b*) Y. Miura and N. Yoshioka, *Chem. – Asian J.*, 2018, **13**, 1683–1687.

4 Y. Hong, J. W. Y. Lam and B. Z. Tang, *Chem. Soc. Rev.*, 2011, **40**, 5361–5388.

5 (*a*) S.-S. Chen, *CrystEngComm*, 2016, **18**, 6543–6565; (*b*) X. Meng, H.-N. Wang, S.-Y. Song and H.-J. Zhang, *Chem. Soc. Rev.*, 2017, **46**, 464–480.

6 (*a*) Z. Song, W. Zhang, M. Jiang, H. H. Sung, R. T. Kwok, H. Nie, I. D. Williams, B. Liu and B. Z. Tang, *Adv. Funct.*

Mater., 2016, **26**, 824–832; (*b*) S. Matsumoto, Y. Zhao and M. Akazome, *Heterocycles*, 2014, **88**, 261–273.

7 Z. Wang, P. Lu, S. Chen, Z. Gao, F. Shen, W. Zhang, Y. Xu, H. S. Kwok and Y. Ma, *J. Mater. Chem.*, 2011, **21**, 5451–5456.

8 Z.-P. Zhuang, M.-P. Kung, A. Wilson, C.-W. Lee, K. Plössl, C. Hou, D. M. Holtzman and H. F. Kung, *J. Med. Chem.*, 2003, **46**, 237–243.

9 B. R. Radziszewski, *Chem. Ber.*, 1877, **10**, 70–75.

10 K. Feng, F.-L. Hsub, D. V. D. Veer, K. Bota and X. R. Bu, *J. Photochem. Photobiol.*, 2004, **165**, 223–228.

11 H. Debus, *Justus Liebigs Ann. Chem.*, 1858, **107**, 199–208.

12 (*a*) F. Bellina, S. Cauteruccio, A. D. Fiore, C. Marchetti and R. Rossi, *Tetrahedron*, 2008, **64**, 6060–6072; (*b*) P.-O. Delaye, M. Pénichon, H. Allouchi, C. Enguehard-Gueiffier and A. Gueiffier, *Org. Biomol. Chem.*, 2017, **15**, 4199–4204; (*c*) M. Lessi, A. Panattoni, L. Guglielmero, P. Minei and F. Bellina, *Synthesis*, 2019, 933–943.

13 (*a*) R. C. Lirag, H. T. M. Le and O. Š. Miljanić, *Chem. Commun.*, 2013, **49**, 4304–4306; (*b*) X.-L. Lu and M. Xia, *J. Mater. Chem. C*, 2016, **4**, 9350–9358.

14 (*a*) S. Ji, J. Yang, Q. Yang, S. Liu, M. Chen and J. Zhao, *J. Org. Chem.*, 2009, **74**, 4855–4865; (*b*) A. G. Crawford, A. D. Dwyer, Z. Liu, A. Steffen, A. Beeby, L.-O. Pålsson, D. J. Tozer and T. B. Marder, *J. Am. Chem. Soc.*, 2011, **133**, 13349–13362; (*c*) H. Maeda, T. Maeda, K. Mizuno, K. Fujimoto, H. Shimizu and M. Inouye, *Chem. – Eur. J.*, 2006, **12**, 824–831.

15 (*a*) Z. Zhao, J. G. Peacock, D. A. Gubler and M. A. Peterson, *Tetrahedron Lett.*, 2005, **46**, 1373–1375; (*b*) A. V. Gulevskaya, A. S. Tyaglivy, A. F. Pozharskii, J. I. Nelina-Nemtseva and D. V. Steglenko, *Org. Lett.*, 2014, **16**, 1582–1585.

16 K. Sonogashira, Y. Tohda and N. Hagiwara, *Tetrahedron Lett.*, 1975, **16**, 4467–4470.

17 C. J. Lovely, H. Du, R. Sivappa, M. R. Bhandari, Y. He and H. V. R. Dias, *J. Org. Chem.*, 2007, **72**, 3741–3749.

18 (*a*) A. Slama-Schwok, M. Blanchard-Desce and J.-M. Lehn, *J. Phys. Chem.*, 1990, **94**, 3894–3902; (*b*) R. Nandy and S. Sankararaman Beilstein, *J. Org. Chem.*, 2010, **6**, 992–1001.

19 C. Reichardt, *Chem. Rev.*, 1994, **94**, 2319–2358.

20 CCDC 1950075(**1a**), 1950076(**1b**), 2025902(**1c**), 1950078(**1d**), 1950077(**1e**), 2025951(**1a**-TFA salt), 2025950(**1d**-TFA salt), and 2025952(**1e**-TFA salt) contain the supplementary crystallographic data for this paper†.

21 (*a*) X. Zhu, Q. Lin, P. Chen, Y.-P. Fu, Y.-M. Zhang, T.-B. Wei New and J. Chem, 2016, **40**, 4562–4565; (*b*) S. Matsumoto, S. Tachibana and M. Akazome, *Heterocycles*, 2020, **100**, 1666–1677.

22 Single crystal of **1b** salt was not obtained by recrystalization, because **1b** was broken in high acidicity of solution. Expected ketone compound is illustrated in Fig. S6 (ESI†).

23 M. J. Frisch, G. W. Trucks, H. B. Schlegel, G. E. Scuseria, M. A. Robb, J. R. Cheeseman, G. Scalmani, V. Barone, B. Mennucci, G. A. Petersson, H. Nakatsuji, M. Caricato, X. Li, H. P. Hratchian, A. F. Izmaylov, J. Bloino, G. Zheng, J. L. Sonnenberg, M. Hada, M. Ehara, K. Toyota, R. Fukuda, J. Hasegawa, M. Ishida, T. Nakajima, Y. Honda, O. Kitao, H. Nakai, T. Vreven, J. A. Montgomery, Jr., J. E. Peralta, F. Ogliaro, M. Bearpark, J. J. Heyd, E. Brothers, K. N. Kudin, V. N. Staroverov, R. Kobayashi, J. Normand, K. Raghavachari, A. Rendell, J. C. Burant, S. S. Iyengar, J. Tomasi, M. Cossi, N. Rega, J. M. Millam, M. Klene, J. E. Knox, J. B. Cross, V. Bakken, C. Adamo, J. Jaramillo, R. Gomperts, R. E. Stratmann, O. Yazyev, A. J. Austin, R. Cammi, C. Pomelli, J. W. Ochterski, R. L. Martin, K. Morokuma, V. G. Zakrzewski, G. A. Voth, P. Salvador, J. J. Dannenberg, S. Dapprich, A. D. Daniels, J. B. Foresman Farkas, J. V. Ortiz, J. Cioslowski and D. J. Fox, *Gaussian 09 (Revision D.01)*, Gaussian, Inc., Wallingford, CT, 2013.

